

# Measurement of Rashba and Dresselhaus spin-orbit magnetic fields

Lorenz Meier<sup>1,2</sup>, Gian Salis<sup>1</sup>, Ivan Shorubalko<sup>2</sup>, Emilio Gini<sup>3</sup>, Silke Schön<sup>3</sup>, Klaus Ensslin<sup>2</sup>

<sup>1</sup>*IBM Research, Zurich Research Laboratory, Säumerstrasse 4, 8803 Rüschlikon, Switzerland*

<sup>2</sup>*Solid State Physics Laboratory, ETH Zurich, 8093 Zurich, Switzerland*

<sup>3</sup>*FIRST Center for Micro- and Nanosciences, ETH Zurich, 8093 Zurich, Switzerland*

(Dated: 15 July 2007)

Spin-orbit coupling is a manifestation of special relativity. In the reference frame of a moving electron, electric fields transform into magnetic fields, which interact with the electron spin and lift the degeneracy of spin-up and spin-down states. In solid-state systems, the resulting spin-orbit fields are referred to as Dresselhaus or Rashba fields, depending on whether the electric fields originate from bulk or structure inversion asymmetry, respectively. Yet, it remains a challenge to determine the absolute value of both contributions in a single sample. Here we show that both fields can be measured by optically monitoring the angular dependence of the electrons' spin precession on their direction of movement with respect to the crystal lattice. Furthermore, we demonstrate spin resonance induced by the spin-orbit fields. We apply our method to GaAs/InGaAs quantum-well electrons, but it can be used universally to characterise spin-orbit interactions in semiconductors, facilitating the design of spintronic devices.

Symmetry-breaking electric fields in semiconductors induce a spin splitting, because electric fields appear to a moving electron as magnetic fields, which interact with the electron spin and couple it with the electron momentum, or wave vector,  $\mathbf{k}$ . In zinc-blende-type crystals, such as GaAs, the electric fields resulting from the lack of an inversion centre lead to bulk inversion asymmetry (BIA) and to the Dresselhaus term in the Hamiltonian [1]. In the conduction band, its coupling is linear or cubic in  $k$  with proportionality constants  $\beta$  and  $\gamma$ , respectively. In heterostructures, additional electric fields are introduced owing to structure inversion asymmetry (SIA), giving rise to the Rashba term [2], which for conduction-band electrons is linear in  $k$  with coupling constant  $\alpha$ . Both contributions have been extensively studied [3], since a potential use of electron spins in future devices (e.g. a spin transistor [4]) requires precise control of the spin's environment and of the Dresselhaus and Rashba fields [5]. Spin-orbit fields also contribute to spin decoherence [6].

In two-dimensional systems, such as quantum wells (QWs), usually  $\alpha \gg \beta$  and  $\gamma \approx 0$  [7, 8, 9, 10]. Therefore, measurements of the spin-orbit coupling initially focused on the Rashba term in QWs and concentrated on the study of beatings in Shubnikov-de-Haas oscillations [8, 10, 11, 12, 13], whose interpretation, however, is debated [14, 15]. More recent experiments include the investigation of antilocalization in magnetotransport [16] or the analysis of photocurrents [17]. In the latter experiment, the ratio  $\alpha/\beta$  could be determined. A gate-induced transition from weak localization to antilocalization allowed the discrimination between Rashba, as well as linear and cubic Dresselhaus contributions to the spin-orbit field [18]. Tuning of the Rashba coupling has been achieved by introducing additional electric fields from gates [9, 19] or by changing the electron density [20, 21].

The influence of effective spin-orbit magnetic fields on optical measurements in a heterostructure was already measured in 1990 [22], and the spin-orbit-induced precession of spin packets was observed more than a

decade later [23, 24]. Remarkably, the in-plane spin-orbit fields in a QW can lead to an out-of-plane spin polarization [25]. In ref. [26], it was pointed out that although spin-orbit and external magnetic fields can be added to describe spin precession [22], a more complicated concept has to be evoked when accounting for the generation of an out-of-plane spin polarization.

In this Article, we show that both Rashba and Dresselhaus fields in the conduction band can be determined by measuring the spin precession of optically polarized electron spins as a function of the direction of their drift momentum. We find good agreement with the assumption that the spins precess about the sum of the effective spin-orbit and an external magnetic field  $\mathbf{B}_0$ . In Sect. I, we derive an expression for the magnitude of this total magnetic field  $B_{\text{tot}}$  as a function of the angles  $\theta$  and  $\varphi$  that  $\mathbf{B}_0$  and the electron drift momentum  $\hbar\mathbf{k}$  include with the crystal's  $[1\bar{1}0]$  axis. These predictions provide a good description of the experimental data  $B_{\text{tot}}(\theta, \varphi)$  of three (001) GaAs/InGaAs QW samples given in Sect. II, and allow us to separately determine the Rashba and Dresselhaus contributions to the spin-orbit field. In Sect. III, we demonstrate spin resonance induced by oscillating spin-orbit fields.

## I. THEORETICAL EXPECTATIONS

Neglecting cubic terms, the Rashba and Dresselhaus spin-orbit couplings in a QW are linear in  $\mathbf{k}$  and can be described by an effective magnetic field [3, 27],

$$\mathbf{B}_{\text{SIA}} = \frac{\alpha}{g\mu_B} \begin{pmatrix} k_y \\ -k_x \end{pmatrix}, \quad \text{and} \quad \mathbf{B}_{\text{BIA}} = \frac{\beta}{g\mu_B} \begin{pmatrix} k_y \\ k_x \end{pmatrix}, \quad (1)$$

for a coordinate system with base vectors  $\hat{\mathbf{x}} \parallel [1\bar{1}0]$  and  $\hat{\mathbf{y}} \parallel [110]$ . Here,  $g$  is the electron's  $g$ -factor and  $\mu_B$  the Bohr magneton. Both fields are in the plane of the QW, but while  $\mathbf{B}_{\text{SIA}}$  is always perpendicular to

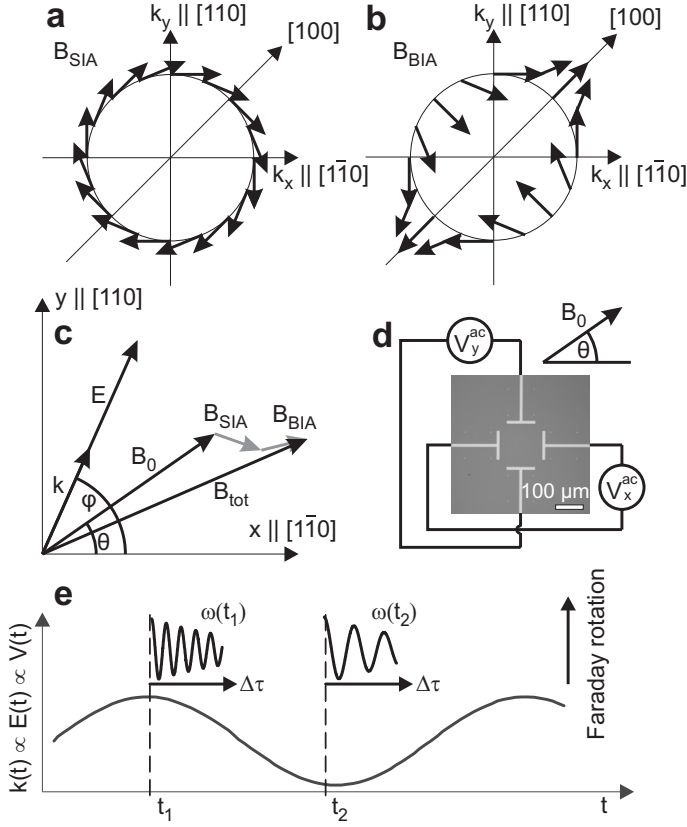


FIG. 1: Orientation of the magnetic and electric fields and measurement setup. **a**, Rashba and **b**, Dresselhaus spin-orbit fields for different orientations of the  $\mathbf{k}$ -vector on a unit circle. **c**, Electric and magnetic fields involved in the experiment. **d**, Optical microscopy image of the sample and wiring of the gates. **e**, The electron precession frequency  $\omega(t)$  is determined at different phases of the oscillating wave vector  $\mathbf{k}(t)$ .

$\mathbf{k}$  (Fig. 1a),  $\mathbf{B}_{\text{BIA}}$  has a different geometrical dependence on  $\mathbf{k}$  (Fig. 1b). A conduction-band electron experiences the total magnetic field  $\mathbf{B}_{\text{tot}} = \mathbf{B}_0 + \mathbf{B}_{\text{SIA}} + \mathbf{B}_{\text{BIA}}$  (Fig. 1c). With a time-dependent  $\mathbf{k}(t) = k_0 \sin(2\pi\nu t) \cdot (\cos\varphi, \sin\varphi)$ , we obtain for the total magnetic field square

$$B_{\text{tot}}^2 = B_0^2 \times \left( 1 + \frac{2k_0 \sin(2\pi\nu t)}{g\mu_B B_0} ([\alpha + \beta] \cos\theta \sin\varphi + [\beta - \alpha] \sin\theta \cos\varphi) + \left( \frac{k_0 \sin(2\pi\nu t)}{g\mu_B B_0} \right)^2 (\alpha^2 + \beta^2 - 2\alpha\beta \cos 2\varphi) \right). \quad (2)$$

$B_{\text{tot}}^2(t)$  is expected to oscillate around  $B_0^2$  with frequencies  $\nu$  and  $2\nu$ . If cubic Dresselhaus terms were included in  $B_{\text{tot}}$ , additional terms proportional to  $k^n$ ,  $n = 3, 4, 6$  would appear in Eq. (2) and induce oscillations at frequencies  $n\nu$ . Assuming that  $|B_{\text{SIA}}|, |B_{\text{BIA}}| \ll B_0$ , we expand the square root of Eq. (2) up to second order in

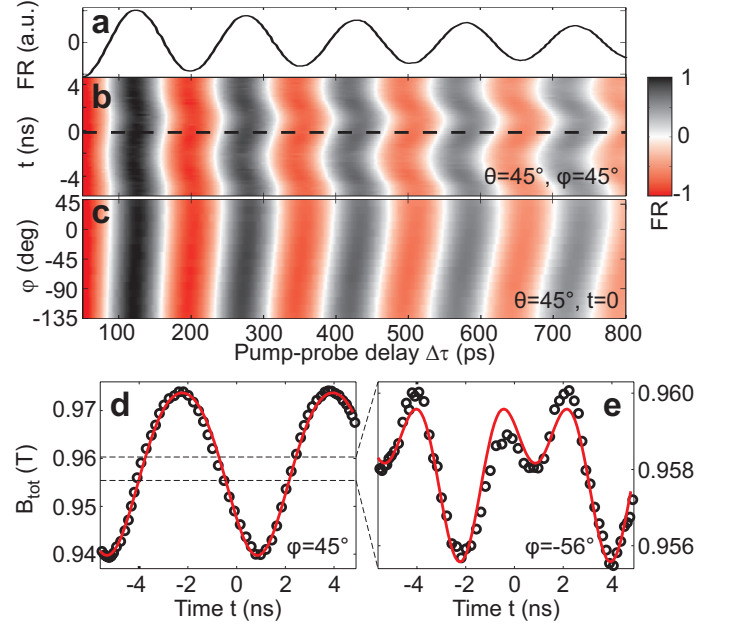


FIG. 2: TRFR signal measured at different times  $t$  and electric field angles  $\varphi$ , at  $\theta = 45^\circ$ . **a**, Faraday rotation vs. pump-probe delay. **b**, TRFR scans at different times  $t$ , the dashed line indicates  $t = 0$ . **c**, TRFR scans at different angles  $\varphi$ , at  $t = 0$ . **d**, **e**, Total magnetic field as a function of  $t$  for **d**,  $\varphi = 45^\circ$  and **e**,  $\varphi = -56^\circ$ . The solid line is a fit to Eq. (3).

$k_0/B_0$ , and obtain, using Eq. (1),

$$B_{\text{tot}}(t) \approx B_0 + A(\theta, \varphi) \sin(2\pi\nu t) + B(\theta, \varphi) \sin^2(2\pi\nu t), \quad (3)$$

with

$$A(\theta, \varphi) = (B_{\text{BIA}} + B_{\text{SIA}}) \cos\theta \sin\varphi + (B_{\text{BIA}} - B_{\text{SIA}}) \sin\theta \cos\varphi, \quad \text{and} \\ B(\theta, \varphi) = [(B_{\text{BIA}} + B_{\text{SIA}}) \sin\theta \sin\varphi - (B_{\text{BIA}} - B_{\text{SIA}}) \cos\theta \cos\varphi]^2 / B_0.$$

By measuring the oscillation amplitude of  $B_{\text{tot}}(t)$  for varying angles  $\theta$  and  $\varphi$ , we can extract the Rashba and Dresselhaus contributions to the spin-orbit magnetic field.

## II. EXPERIMENTS

To induce an oscillating spin-orbit field, we impose an oscillating drift momentum  $\hbar\mathbf{k}(t)$  on the QW electrons by applying an in-plane a.c. electric field  $\mathbf{E}(t) = \mathbf{E}_0 \sin(2\pi\nu t)$ ,  $\nu = 160$  MHz, at an angle  $\varphi$  with the  $x$ -axis, see Fig. 1c. In the diffusive limit, electron scattering occurs fast on the timescale  $1/\nu$ , and  $\mathbf{k}(t) \propto \mathbf{E}(t)$  (see Methods). We monitor the spin precession frequency  $\omega(t) = g\mu_B B_{\text{tot}}(t)/\hbar$  of optically polarized electron spins at different times  $t$  (see Fig. 1e) using time-resolved Faraday rotation (TRFR, see Methods).

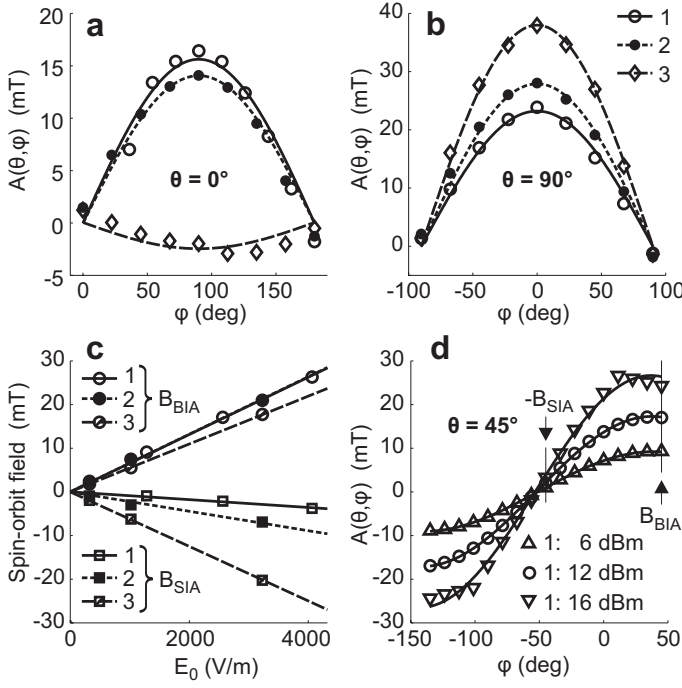


FIG. 3: Spin-orbit fields as a function of  $\varphi$  for  $\theta = 0, 90^\circ$  and  $45^\circ$ . Depending on  $\theta$ , we measure **a**,  $(B_{\text{BIA}} + B_{\text{SIA}}) \sin \varphi$  [at  $\theta = 0$ ] or **b**,  $(B_{\text{BIA}} - B_{\text{SIA}}) \cos \varphi$  [at  $\theta = 90^\circ$ ]. The gate modulation amplitude was 12 dBm for sample 1 and 14 dBm for samples 2 and 3. **c**, Both  $B_{\text{SIA}}$  and  $B_{\text{BIA}}$  increase linearly as a function of the electric field. **d**, For  $\theta = 45^\circ$ , the measured spin-orbit field is  $B_{\text{BIA}} \cos(\varphi - \pi/4) + B_{\text{SIA}} \sin(\varphi - \pi/4)$  with a linear dependence on the applied gate voltage. At  $\varphi = 45^\circ$ , we directly measure  $B_{\text{BIA}}$ , and at  $\varphi = -45^\circ$ ,  $-B_{\text{SIA}}$ .

Figure 2b shows TRFR oscillations at different  $t$ . Owing to the oscillating spin-orbit field,  $\omega(t)$  and consequently  $B_{\text{tot}}(t)$  change periodically with  $t$ . Likewise,  $\omega(t)$  changes with the angle  $\varphi$  (Fig. 2c), as predicted by Eq. (3). The fit to this equation with  $B_0$ ,  $A(\theta, \varphi)$ , and  $B(\theta, \varphi)$  as fit parameters matches the data points very well (Fig. 2d), with  $B_0 = 0.958$  T, in agreement with Hall probe measurements of the external magnetic field. For most  $\varphi$ , we find  $A \gg B$ . The quadratic term in  $k(t)$ ,  $B(\theta, \varphi)$ , which contributes to oscillations with frequency  $2\nu$ , is visible in the experiment only when rotating  $\mathbf{E}$  to an angle  $\varphi$  at which the  $k$ -linear term  $A(\theta, \varphi)$  is weak, see Fig. 2e. Apart from the geometrical dependence, the amplitude of  $B(\theta, \varphi)$  is suppressed by a factor  $(|B_{\text{BIA}}| + |B_{\text{SIA}}|)/B_0 \approx 0.03$ , i.e. by more than one order of magnitude compared with  $A(\theta, \varphi)$ . Higher-order contributions were below the detection limit (roughly 1/4 of the second-order effects), which indicates that in our samples, *cubic* Dresselhaus terms are not relevant.

Given that already second-order terms are strongly suppressed, we restrict our analysis to the linear term  $A(\theta, \varphi)$ . For  $\theta = 0$  and  $90^\circ$ ,  $A(\theta, \varphi)$  is given by  $(B_{\text{SIA}} + B_{\text{BIA}}) \sin \varphi$  and  $(B_{\text{BIA}} - B_{\text{SIA}}) \cos \varphi$ , respectively. This dependence is observed in the experiment, as shown in Fig. 3a and b. The measured data points

clearly follow  $\sin \varphi$  for  $\theta = 0$  and  $\cos \varphi$  for  $\theta = 90^\circ$  (solid lines). From the two measurements at  $\theta = 0$  and  $90^\circ$ , we can extract the spin-orbit magnetic fields  $B_{\text{SIA}}$  and  $B_{\text{BIA}}$ . Normalized to a gate modulation amplitude of  $V_0 = 2$  V ( $\approx 13$  dBm), corresponding to an electric field of  $E_0 \approx 2,900$  V/m, we find  $B_{\text{SIA}} = -4.2, -8.5$ , and  $-17.6$  mT and  $B_{\text{BIA}} = 21.6, 21.1$ , and  $15.7$  mT for samples 1, 2, and 3, respectively. Note that as  $t$  is known up to an offset  $t_0$ , the sign of  $A(\theta, \varphi)$  is arbitrary, leading to an uncertainty in the absolute sign of  $B_{\text{SIA}}$  and  $B_{\text{BIA}}$  (the relative sign is obtained). We choose  $B_{\text{BIA}} > 0$ . As a function of the magnitude of the applied electric field  $E_0$ ,  $B_{\text{SIA}}$  and  $B_{\text{BIA}}$  increase linearly (see Fig. 3c), as expected from the linear relation between  $k(t)$  and  $E(t)$  and Eq. (1). We have conducted the same measurements at different magnitudes of  $B_0 = 0.55$  and  $0.82$  T, and found similar values for the spin-orbit fields.

As discussed above, measurements at two angles,  $\theta = 0$  and  $90^\circ$ , were needed to obtain  $B_{\text{SIA}}$  and  $B_{\text{BIA}}$ . At  $\theta = 45^\circ$  both  $B_{\text{SIA}}$  and  $B_{\text{BIA}}$  can be determined simultaneously. This is because not only the amplitude, but also the phase of the oscillation in  $\varphi$  contains information about the spin-orbit fields. The zero-crossing occurs at  $\varphi_0 = \arctan[(B_{\text{SIA}} - B_{\text{BIA}})/(B_{\text{SIA}} + B_{\text{BIA}})]$ , compared with  $\varphi_0 = \theta$  for  $\theta = 0$  and  $90^\circ$ . For  $\theta = \varphi = 0$  and  $90^\circ$ ,  $\mathbf{B}_{\text{SIA}}$  and  $\mathbf{B}_{\text{BIA}}$  are perpendicular to  $\mathbf{B}_0$  (Fig. 1a and b) and  $A(\theta, \varphi)$  vanishes, because it is equal to the component of  $\mathbf{B}_{\text{SIA}} + \mathbf{B}_{\text{BIA}}$  along the direction of  $\mathbf{B}_0$ . If however  $\theta = \varphi = 45^\circ$ ,  $\mathbf{B}_{\text{SIA}}$  still is perpendicular to  $\mathbf{B}_0$ , but  $\mathbf{B}_{\text{BIA}}$  is now parallel, and  $A(\theta, \varphi) = B_{\text{BIA}}$ .

The measurement at  $\theta = 45^\circ$  is shown in Fig. 3d, with a fit to Eq. (3). For  $V_0 = 2$  V, we extract the spin-orbit fields  $B_{\text{SIA}} = -2.4$  mT and  $B_{\text{BIA}} = 19.1$  mT for sample 1. These values correspond well to the values obtained from  $\theta = 0$  and  $90^\circ$ . Relative variations in  $B_{\text{SIA}}$  of up to 50% (but far less in  $B_{\text{BIA}}$ ) occurred for different cool-downs of the same sample, which we attribute to the freezing of electron states in the QW interface or to strain.

Knowing the electron  $g$ -factor and drift wave vector  $k$ , we can calculate the coupling constants  $\alpha$  and  $\beta$  from  $B_{\text{SIA}}$  and  $B_{\text{BIA}}$  using Eq. (1). For sample 3, the mobility is known (see Methods), and with a numerical simulation of  $E_0$ , we obtain  $\alpha = \hbar g \mu_B B_{\text{SIA}} / m^* \mu E_0 = 1.5 \times 10^{-13}$  eV·m and  $\beta = \hbar g \mu_B B_{\text{BIA}} / m^* \mu E_0 = -1.4 \times 10^{-13}$  eV·m, where we have used  $g = -0.27$ , as independently measured by TRFR in a known external magnetic field, and assuming  $g < 0$ . Previous experiments report  $\alpha \approx 5 - 10 \times 10^{-12}$  eV·m on  $\text{In}_{0.53}\text{Ga}_{0.47}\text{As}/\text{In}_{0.52}\text{Al}_{0.48}\text{As}$  QWs or heterostructures [9, 13, 16] and in  $\text{InAs}/\text{AlSb}$  QWs [20] and assume  $\alpha \gg \beta$ . The Rashba coupling is proportional to the average electric field in the *valence* band [3], including contributions from band discontinuities. We estimate the valence band offset in our QWs to be on the order of 10 meV, which is much smaller than in those previously investigated structures, and explains our small value of  $\alpha$ . Our  $\alpha$  is about four times larger than that reported in ref. [23], where an  $\text{In}_{0.07}\text{GaAs}$  epilayer (10 times thicker than our QW) was studied. There, the

interfaces play a minor role and strain-induced spin-orbit coupling predominates. The linear Dresselhaus term is expected to scale with the extent of the wave function in the confinement direction,  $\langle k_z^2 \rangle$ . For an infinitely deep well with width  $\ell$ ,  $k_z \propto 1/\ell$ , and  $\beta \propto 1/\ell^2$ . Assuming that samples 1 and 2 have similar mobilities, we observed almost the same  $\beta$ , even though the QW in sample 2 is twice as wide as that in sample 1. This could be attributed to inhomogeneous In deposition during growth, leading to a triangular confinement potential, where the nominal QW width has less influence on  $\beta$ .

### III. ELECTRIC-DIPOLE-INDUCED SPIN RESONANCE

In electron spin resonance (ESR) experiments, spins that are initially polarized along the direction of a static magnetic field  $B_0 = B_z$  perform Rabi oscillations between the states parallel and anti-parallel to  $B_z$  if an a.c. magnetic field (the tipping field) is applied in the plane perpendicular to  $B_z$  and at the Larmor frequency  $\nu = g\mu_B B_z/h$ . Instead of an a.c. magnetic field, we use an a.c. electric field  $E_x(t)$  in the plane of the QW. It induces an oscillating spin-orbit field  $B_y(t)$ , which can serve as a tipping field for ESR, in this context referred to as electric-dipole-induced spin resonance (EDSR) [28]. The measurements presented in Fig. 4 have been conducted in Faraday geometry with sample 1. Here, the external magnetic field  $B_z$  is parallel to the laser propagation and perpendicular to the QW plane. The pump laser pulse polarizes the spins into an eigenstate, in line with  $B_z$ , and the probe pulse monitors the spin polarization along  $z$ . In Fig. 4a, the pump-probe delay  $\Delta\tau$  has been set to 3 ns, and the Faraday signal is recorded while sweeping the frequency  $\nu$  of  $E_x(t)$  and  $B_z$ . On resonance, the optically generated spin polarization precesses about the spin-orbit-induced tipping field, and the TRFR signal at  $\Delta\tau = 3$  ns becomes negative. We observe spin resonance with  $|g| = 0.57$ , which is in agreement with the observed spin precession in Sect. II.

In Fig. 4b and c, TRFR scans are collected for varying  $B_z$ , monitoring the spin dynamics. At  $B_z = 120$  mT, the Larmor frequency matches the electric field frequency  $\nu = 960$  MHz and resonance occurs. Note that the short spin relaxation time of  $\approx 1$  ns strongly reduces the signal. At  $\Delta\tau_s \approx 1800$  ps, the spins have performed a  $\pi/2$  Rabi oscillation, yielding an estimate of the tipping field amplitude  $B_y = 2h/g\mu_B 4\Delta\tau_s \approx 35$  mT. Here, the factor 2 takes into account the linearly (and not circularly) oscillating tipping field [29]. This value agrees well with the measurements of  $|\mathbf{B}_{\text{SIA}} - \mathbf{B}_{\text{BIA}}| \approx 33$  mT at a gate modulation amplitude of  $V_0 \approx 2.5$  V (15 dBm) and  $\varphi = 0$ .

In ESR, one assumes a tipping field that oscillates circularly in the  $x/y$  plane, resulting in a monotonous decrease of the spin polarization along  $z$  during the first  $\pi/2$  Rabi oscillation. The spin dynamics can then be solved analytically in the “rotating frame”. In EDSR,

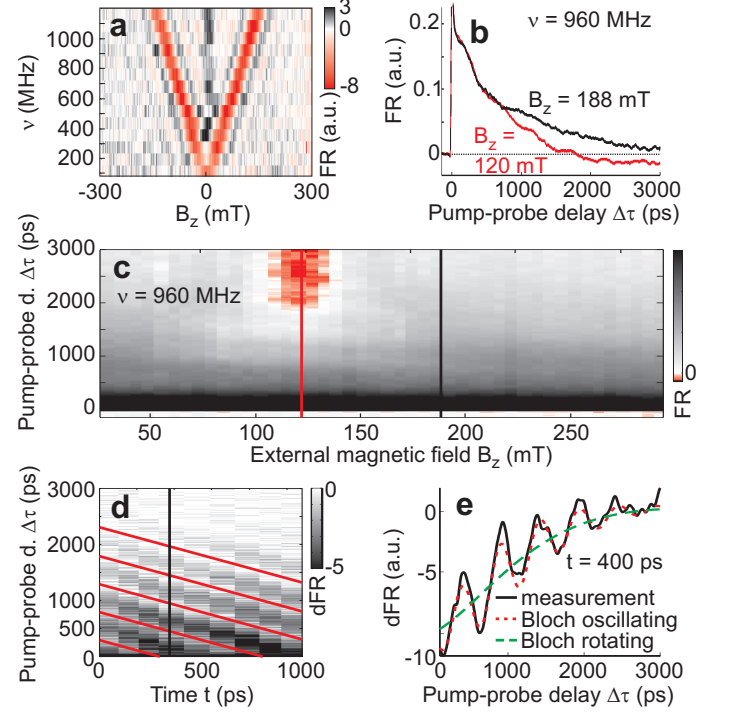


FIG. 4: Spin resonance induced by an oscillating spin-orbit field. **a**, TRFR signal at  $\Delta\tau = 3$  ns for varying external magnetic fields  $B_z$  and electric field frequencies  $\nu$ . Resonance is observed with  $|g| = 0.57$ . **b**, TRFR scans on (red line) and off (black line) resonance. **c**, TRFR scans  $\Theta_F(\Delta\tau)$  at different  $B_z$ . On resonance, the spins precess coherently about the spin-orbit induced-tipping field. **d**, Differential TRFR signal  $\Theta_F(\Delta\tau + t)$  on resonance ( $\nu = 960$  MHz), red lines are guides to the eye at  $\Delta\tau = t$ . **e**, Measured  $\Theta_F(\Delta\tau) \propto \dot{S}_z(\Delta\tau)$  (solid line) and Bloch simulations with linearly oscillating (dotted) and rotating tipping field (dashed), at  $\nu = 960$  MHz and  $t = 400$  ps (solid line in **d**).

the Rabi oscillation on resonance is not steady with time (Fig. 4b), because the tipping field oscillates linearly on the  $y$ -axis instead. The precession of a spin is described by the Bloch equations (neglecting spin relaxation)

$$\dot{\mathbf{S}} = \frac{g\mu_B}{\hbar} \mathbf{B} \times \mathbf{S}, \quad (4)$$

from which we find  $\dot{S}_z(t') = g\mu_B B_y(t') S_x(t')/\hbar$ , where the dot denotes the time derivative and  $t' = \Delta\tau + t$ . The tipping field  $B_y(t') \propto \sin(2\pi\nu t')$  and with it  $\dot{S}_z(t')$  vanish twice per electric field period  $1/\nu$ , resulting in a stepwise decrease of  $S_z$  (on resonance,  $S_x(t')$  and  $B_y(t')$  vanish simultaneously). This is shown in Fig. 4d, where the time derivative of the Faraday signal  $\dot{\Theta}_F(t') \propto \dot{S}_z(t')$  is plotted for different  $\Delta\tau$  and  $t$  and for  $B_z$  on resonance. Apart from decaying with time, it is periodic in both  $\Delta\tau$  and  $t$ , with period  $1/2\nu$ . The stepwise decrease of  $S_z$  can be reproduced by a numerical solution of the Bloch equations including a spin-relaxation term with  $T_1 = T_2 = 1$  ns,  $B_z = 120$  mT,  $B_x = 0$  and  $B_y(t) = 34$  mT  $\sin(2\pi\nu t)$ .

We show  $\dot{S}_z$  of this solution in Fig. 4e, together with the experimentally measured  $\Theta_F(t')$  and the corresponding solution with a rotating tipping field. For the latter, the tipping field has to be reduced by a factor 2 [29].

The technique presented here to unambiguously determine Rashba and Dresselhaus spin-orbit fields with high precision can be extended to any semiconductor sample, if optical access to electron spin precession is provided. This is useful for the optimization of semiconductor materials and QW designs with increased spin-orbit fields that can be used for efficient EDSR-based spin manipulation. Moreover, it might facilitate the tuning of systems where Rashba and Dresselhaus terms cancel out each other, opening an avenue to study spin dynamics in this interesting regime.

## IV. METHODS

### A. Application of the electric field

In the centre of four top-gate electrodes, which enclose a square with 150  $\mu\text{m}$  side length (see Fig. 1d), the angle  $\varphi$  of the oscillating electric field  $\mathbf{E}(t)$  is determined by the amplitudes  $E_x$  and  $E_y$  of two superposed fields along  $\hat{\mathbf{x}}$  and  $\hat{\mathbf{y}}$ ,  $\mathbf{E}_0 = E_x\hat{\mathbf{x}} + E_y\hat{\mathbf{y}}$ .  $E_x$  and  $E_y$  are generated by two phase-locked oscillators, each driving two opposite electrodes. In the diffusive regime, the scattering time of the electrons in the QW ( $\approx 0.5$  ps from mobility measurements) is much smaller than  $1/\nu$  and, therefore, their average drift wave vector points along  $\mathbf{E}(t)$  and its magnitude is given by  $k(t) = m^*\mu E(t)/\hbar = m^*\mu E_0 \sin(2\pi\nu t)/\hbar$ , with  $m^*$  the electron effective mass,  $\mu$  the electron mobility in the QW, and  $\hbar$  Planck's constant.

### B. Time-resolved Faraday rotation

To determine the total magnetic field acting on the QW electrons in the centre of the four top-gate electrodes (see Fig. 1d), we employ time-resolved Faraday rotation (TRFR) [30]. A first, circularly polarized laser pulse ( $P = 400$   $\mu\text{W}$ , focus diameter  $\approx 15$   $\mu\text{m}$ , pulse width  $\approx 3$  ps) tuned to the absorption edge of the QW (870 nm) creates a spin polarization perpendicular to the QW plane. The linear polarization of a second laser pulse ( $P = 50$   $\mu\text{W}$ ), which is transmitted through the sam-

ple at a time delay  $\Delta\tau$  with respect to the first pulse, is rotated by an angle  $\Theta_F$  proportional to the spin polarization along the QW normal. As the spins precess about a local in-plane magnetic field  $\mathbf{B}_{\text{tot}}$ , an oscillating signal  $\Theta_F(\Delta\tau) = \Theta_0 \cos(\omega\Delta\tau)e^{-\Delta\tau/T_2^*}$  is measured (see Fig. 2a). The exponential accounts for the finite spin lifetime  $T_2^*$ , and  $\omega = g\mu_B B_{\text{tot}}/\hbar$  is proportional to the magnitude of the total magnetic field  $\mathbf{B}_{\text{tot}}$ . Experiments are performed at  $T = 40$  K, where effects of nuclear polarization are negligible [31]. To probe the spin precession at a given time  $t$  and thus at a given phase of  $k(t) \propto E(t)$ , the pulsed laser is phase-locked to the oscillatory field  $E(t)$  with a variable phase shift. We probe the spin precession during an interval  $\Delta\tau = 0 \dots 700$  ps, which is much shorter than the a.c. electric field period of  $1/\nu = 6,250$  ps. Therefore,  $\mathbf{E}(t)$  is roughly constant over the spin precession observed and a well-defined precession frequency  $\omega(t)$  can be obtained, see Fig. 1e. For experimental reasons, the time  $t$  is known up to an offset  $t_0$ , which is constant throughout the experiment.

### C. Sample structure

Sample 1 is a 20-nm-wide GaAs/InGaAs QW with an In content of 8.5%, capped by 21 nm GaAs and grown on a GaAs substrate by metal organic chemical vapor deposition. Both cap and well are  $n$ -doped to maximize the spin lifetime [32]. Sample 2 is similar to sample 1, but with a QW width of 43 nm. Sample 3 is a GaAs/InGaAs QW with an In content aimed at 10%, grown by molecular beam epitaxy,  $n$ -doped on both sides and in the 20-nm-wide QW, and capped by 30 nm GaAs. For this sample, we determined a carrier density  $n_s = 5.8 \times 10^{11} \text{ cm}^{-2}$  and a mobility  $\mu = 10,600 \text{ cm}^2/\text{Vs}$  in a Van-der-Pauw Hall measurement. Transport measurements of samples 1 and 2 were dominated by strongly localized states, presumably due to a parallel conductivity from the doping layer, and rendered a determination of  $n_s$  and  $\mu$  in the QW impossible. In the optical measurements, however, the QW could be probed independently of the doping layer. The fitting parameter  $B_0$  in Eq. (3) is independent of  $\theta$  for all three samples, which indicates that the  $g$ -factor is isotropic in the QW plane, as expected for (001) GaAs/InGaAs QWs. Top-gate electrodes are fabricated by evaporating 80 nm Au on a PMMA mask defined by standard electron-beam lithography techniques.

- 
- [1] Dresselhaus, G. Spin-orbit coupling effects in zinc blende structures. *Phys. Rev.* **100**, 580–586 (1955).
  - [2] Bychkov, Y. A. & Rashba, E. I. Oscillatory effects and the magnetic susceptibility of carriers in inversion layers. *J. Phys. C* **17**, 6039–6045 (1984).
  - [3] Winkler, R. *Spin-Orbit Coupling Effects in Two-Dimensional Electron and Hole Systems*, vol. 191/2003

of *Springer Tracts in Modern Physics* (Springer, Berlin, 2003).

- [4] Datta, S. & Das, B. Electronic analog of the electro-optic modulator. *Appl. Phys. Lett.* **56**, 665–667 (1990).
- [5] Schliemann, J., Egues, J. C. & Loss, D. Nonballistic spin-field-effect transistor. *Phys. Rev. Lett.* **90**, 146801 (2003).



- [6] D'Yakonov, M. I. & Perel', V. I. Spin relaxation of conduction electrons in noncentrosymmetric semiconductors. *Sov. Phys. Solid State* **13**, 3023–3026 (1971).
- [7] Lommer, G., Malcher, F. & Rossler, U. Spin splitting in semiconductor heterostructures for  $B \rightarrow 0$ . *Phys. Rev. Lett.* **60**, 728–731 (1988).
- [8] Luo, J., Munekata, H., Fang, F. F. & Stiles, P. J. Effects of inversion asymmetry on electron energy band structures in GaSb/InAs/GaSb quantum wells. *Phys. Rev. B* **41**, 7685–7693 (1990).
- [9] Nitta, J., Akazaki, T., Takayanagi, H. & Enoki, T. Gate control of spin-orbit interaction in an inverted  $\text{In}_{0.53}\text{Ga}_{0.47}\text{As}/\text{In}_{0.52}\text{Al}_{0.48}\text{As}$  heterostructure. *Phys. Rev. Lett.* **78**, 1335–1338 (1997).
- [10] Schapers, T. *et al.* Effect of the heterointerface on the spin splitting in modulation doped  $\text{In}_x\text{Ga}_{1-x}\text{As}/\text{InP}$  quantum wells for  $B \rightarrow 0$ . *J. Appl. Phys.* **83**, 4324–4333 (1998).
- [11] Das, B. *et al.* Evidence for spin splitting in  $\text{In}_x\text{Ga}_{1-x}\text{As}/\text{In}_{0.52}\text{Al}_{0.48}\text{As}$  heterostructures as  $B \rightarrow 0$ . *Phys. Rev. B* **39**, 1411–1414 (1989).
- [12] Engels, G., Lange, J., Schäpers, T. & Lüth, H. Experimental and theoretical approach to spin splitting in modulation-doped  $\text{In}_x\text{Ga}_{1-x}\text{As}/\text{InP}$  quantum wells for  $B \rightarrow 0$ . *Phys. Rev. B* **55**, R1958–R1961 (1997).
- [13] Hu, C.-M. *et al.* Zero-field spin splitting in an inverted  $\text{In}_{0.53}\text{Ga}_{0.47}\text{As}/\text{In}_{0.52}\text{Al}_{0.48}\text{As}$  heterostructure: Band nonparabolicity influence and the subband dependence. *Phys. Rev. B* **60**, 7736–7739 (1999).
- [14] Pfeffer, P. & Zawadzki, W. Spin splitting of conduction subbands in III-V heterostructures due to inversion asymmetry. *Phys. Rev. B* **59**, R5312–R5315 (1999).
- [15] Brosig, S. *et al.* Zero-field spin splitting in InAs/AlSb quantum wells revisited. *Phys. Rev. B* **60**, R13989–R13992 (1999).
- [16] Koga, T., Nitta, J., Akazaki, T. & Takayanagi, H. Rashba spin-orbit coupling probed by the weak antilocalization analysis in InAlAs/InGaAs/InAlAs quantum wells as a function of quantum well asymmetry. *Phys. Rev. Lett.* **89**, 046801 (2002).
- [17] Ganichev, S. D. *et al.* Experimental separation of Rashba and Dresselhaus spin splittings in semiconductor quantum wells. *Phys. Rev. Lett.* **92**, 256601 (2004).
- [18] Miller, J. B. *et al.* Gate-controlled spin-orbit quantum interference effects in lateral transport. *Phys. Rev. Lett.* **90**, 076807 (2003).
- [19] Grundler, D. Large Rashba splitting in InAs quantum wells due to electron wave function penetration into the barrier layers. *Phys. Rev. Lett.* **84**, 6074–6077 (2000).
- [20] Heida, J. P., van Wees, B. J., Kuipers, J. J., Klapwijk, T. M. & Borghs, G. Spin-orbit interaction in a two-dimensional electron gas in a InAs/AlSb quantum well with gate-controlled electron density. *Phys. Rev. B* **57**, 11911–11914 (1998).
- [21] Matsuyama, T., Kürsten, R., Meißner, C. & Merkt, U. Rashba spin splitting in inversion layers on  $p$ -type bulk InAs. *Phys. Rev. B* **61**, 15588–15591 (2000).
- [22] Kalevich, V. & Korenev, V. Effect of electric field on the optical orientation of 2D electrons. *JETP Lett.* **52**, 230–235 (1990).
- [23] Kato, Y., Myers, R. C., Gossard, A. C. & Awschalom, D. D. Coherent spin manipulation without magnetic fields in strained semiconductors. *Nature* **427**, 50–53 (2004).
- [24] Crooker, S. A. & Smith, D. L. Imaging spin flows in semiconductors subject to electric, magnetic, and strain fields. *Phys. Rev. Lett.* **94**, 236601 (2005).
- [25] Kato, Y. K., Myers, R. C., Gossard, A. C. & Awschalom, D. D. Current-induced spin polarization in strained semiconductors. *Phys. Rev. Lett.* **93**, 176601 (2004).
- [26] Engel, H.-A., Rashba, E. I. & Halperin, B. I. Out-of-plane spin polarization from in-plane electric and magnetic fields. *Phys. Rev. Lett.* **98**, 036602 (2007).
- [27] Ganichev, S. & Prettl, W. Spin photocurrents in quantum wells. *J. Phys.: Condens. Matter* **15**, R935–R983 (2003).
- [28] Duckheim, M. & Loss, D. Electric-dipole-induced spin resonance in disordered semiconductors. *Nature Phys.* **2**, 195–199 (2006).
- [29] Bloch, F. & Siegert, A. Magnetic resonance for nonrotating fields. *Phys. Rev.* **57**, 522–527 (1940).
- [30] Crooker, S. A., Awschalom, D. D. & Samarth, N. Time-resolved faraday rotation spectroscopy of spin dynamics in digital magnetic heterostructures. *IEEE J. Sel. Top. Quantum Electron.* **1**, 1082–1092 (1995).
- [31] Meier, L., Salis, G., Ellenberger, C., Ensslin, K. & Gini, E. Stray-field-induced modification of coherent spin dynamics. *Appl. Phys. Lett.* **88**, 172501 (2006).
- [32] Kikkawa, J. M. & Awschalom, D. D. Resonant spin amplification in  $n$ -type GaAs. *Phys. Rev. Lett.* **80**, 4313–4316 (1998).

## V. ADDENDUM

### A. Correspondence

Correspondence and requests for materials should be addressed to L.M. (meier.lorenz@phys.ethz.ch) or G.S. (gsa@zurich.ibm.com).

### B. Acknowledgements

The authors wish to acknowledge R. Leturcq for help with sample preparation and M. Duckheim, D. Loss, R. Allenspach and T. Ihn for discussions. This work was supported by the Swiss National Science Foundation (NCCR Nanoscale Science).

### C. Author contributions

L.M. performed the experiments and analysed the data in close collaboration with G.S. Samples were fabricated by L.M. and I.S., and grown by E.G. (samples 1 and 2) and S.S. (sample 3). K.E. initiated the collaboration and supported the project in discussions.

### D. Competing Interests

The authors declare that they have no competing financial interests.